Monthly Notices of the ROYAL ASTRONOMICAL SOCIETY

MNRAS **528,** 5880–5889 (2024) https://doi.org/10.1093/mnras/stad4002
Advance Access publication 2024 January 11

Gaia GraL: *Gaia* DR2 gravitational lens systems – VIII. A radio census of lensed systems

Dougal Dobie [1,2]★ Dominique Sluse,[3] Adam Deller [1,2] Tara Murphy [2,4] Alberto Krone-Martins,[5,6] Daniel Stern,[7] Ziteng Wang [2,4] Yuanming Wang [1,2] Céline Bœhm,[4] S. G. Djorgovski,[8] Laurent Galluccio,[9] Ludovic Delchambre,[3] Thomas Connor,[7,10] Jakob Sebastiaan den Brok [10] Pedro H. Do Vale Cunha,[11] Christine Ducourant,[12] Matthew J. Graham [8] Priyanka Jalan,[13] Sergei A. Klioner,[14] Jonas Klüter,[15] François Mignard,[9] Vibhore Negi [16] Quentin Petit,[12] Sergio Scarano, Jr,[17] Eric Slezak,[9] Jean Surdej,[3] Ramachrisna Teixeira,[11] Dominic J. Walton[18] and Joachim Wambsganss[19]

Affiliations are listed at the end of the paper

Accepted 2023 December 15. Received 2023 December 14; in original form 2023 November 13

ABSTRACT

We present radio observations of 24 confirmed and candidate strongly lensed quasars identified by the *Gaia* Gravitational Lenses working group. We detect radio emission from eight systems in 5.5 and 9 GHz observations with the Australia Telescope Compact Array (ATCA), and 12 systems in 6 GHz observations with the Karl G. Jansky Very Large Array (VLA). The resolution of our ATCA observations is insufficient to resolve the radio emission into multiple lensed images, but we do detect multiple images from 11 VLA targets. We have analysed these systems using our observations in conjunction with existing optical measurements, including measuring offsets between the radio and optical positions for each image and building updated lens models. These observations significantly expand the existing sample of lensed radio quasars, suggest that most lensed systems are detectable at radio wavelengths with targeted observations, and demonstrate the feasibility of population studies with high-resolution radio imaging.

Key words: gravitational lensing: strong – radio continuum: general.

1 INTRODUCTION

Strong gravitational lens systems allow us to investigate a number of astrophysical phenomena, including dark matter haloes and galaxy substructure, and also allow one-step measurement of the Hubble constant. These studies have historically been limited by the small number of known lenses, as their discovery requires imaging with both high sensitivity and resolution, which is impractical to carry out over large areas of the sky with most telescopes. However, this has changed with the launch of the *Gaia* satellite, which is carrying out an all-sky survey with high sensitivity ($G \sim 20.7$ mag) and microarcsecond astrometric precision. The *Gaia* Gravitational Lenses working group (GraL) searches for multiply imaged lensed quasars in *Gaia* data by applying machine learning techniques to *Gaia* observations (Krone-Martins et al. 2018; Delchambre et al. 2019). The most promising candidates are then confirmed via spectroscopic follow-up (Wertz et al. 2019; Stern et al. 2021).

Radio observations provide a number of contributions to the strong gravitational lens modelling effort. Their primary utility is being minimally affected by gravitational microlensing and dust obscuration (Wambsganss 1990, 2006). In addition, the detection of radio emission from a lens enables follow-up with Very Long Baseline Interferometry (VLBI). The milliarcsecond resolution imaging obtained with VLBI can be used to model the mass distribution (including detecting substructure) of the lensing galaxy both via the microarcsecond-precision relative astrometry it provides, and by its ability to resolve structure in the lensed components (Suyu et al. 2012; MacLeod et al. 2013; Hsueh et al. 2020; Powell et al. 2022). Radio observations can also be used to place independent constraints on lens time delays through monitoring of the total flux from each image, along with the polarization properties of that emission (Biggs 2021, and references therein).

The largest single collection of radio lensed quasars is from the Cosmic Lens All-Sky Survey. The sample consists of 22 systems (9 quadruply imaged and 12 doubly imaged) with a flux density limit of 30 mJy (Browne et al. 2003). While only ~ 10 per cent of the quasar population is radio-loud[1] (e.g. Kellermann et al. 2016), it is possible to detect intrinsically faint lensed radio emission from quasars (Jackson et al. 2015; Hartley et al. 2019, 2021; Mangat et al. 2021). This paper presents a pilot radio survey of 24 additional lensed

★ E-mail: ddobie@swin.edu.au

[1]Definitions of 'radio-loud' vary, but typically require $L_{\rm radio} \gtrsim 10^{23}$ W Hz^{-1}.

Table 1. Overview of the systems observed in this work. Results of the observations can be found in Table 2 (lenses with Declination < -10 deg observed with the ATCA) and Table 3 (the remaining lenses observed with the VLA).

Lens	Type	Reference
GRAL J022958.17+032032.1	Double	Krone-Martins et al. (2019)
GRAL J024612.2−184505.2	Double	Krone-Martins et al. (2019)
GRAL J024848742+191330571	Quad	Delchambre et al. (2019)
GRAL J034611.0+215444.8	Double	Krone-Martins et al. (2019)
GRAL J053036992−373011003	Quad	Delchambre et al. (2019)
GRAL J060710888−215218058	Quad	Stern et al. (2021)
GRAL J060841.42+422936.87	Quad	Stern et al. (2021)
GRAL J065904.0+162908.6	Quad	Delchambre et al. (2019)
GRAL J081828298−261325078	Quad	Stern et al. (2021)
GRAL J081830.4+060137.8	Double	Krone-Martins et al. (2019)
GRAL J085911925−301134907	Double	Unpublished (candidate)
GRAL J090710.5+000321.2	Double	Krone-Martins et al. (2019)
GRAL J113100−441959	Quad	Krone-Martins et al. (2018)
GRAL J125955.5+124152.4	Double	Krone-Martins et al. (2019)
GRAL J153725327−301017053	Quad	Stern et al. (2021)
GRAL J155656.380−135217.292	Double	Krone-Martins et al. (2019)
GRAL J165105371−041724936	Quad	Stern et al. (2021)
GRAL J181730853+272940139	Quad	Stern et al. (2021)
GRAL J201454.1−302452.1	Double	Stern et al. (2021)
GRAL J201749.0+620443.5	Quad	Stern et al. (2021)
GRAL J203802−400815	Quad	Krone-Martins et al. (2018)
GRAL J210328980−085049486	Quad	Stern et al. (2021)
GRAL J220015.55+144859.5	Double	Krone-Martins et al. (2019)
GRAL J234330.6+043558.0	Double	Krone-Martins et al. (2019)

systems detected at optical wavelengths by the GraL collaboration using the Australia Telescope Compact Array (ATCA) and the Karl G. Jansky Very Large Array (VLA). Of particular note is our detection of radio emission from twelve quadruply imaged systems (of which half are resolved into individual images), almost doubling the number of quadruply imaged systems with detected radio emission.

2 OBSERVATIONS AND DATA REDUCTION

We carried out radio observations of all GraL confirmed and candidate lenses discovered as of 2019 December as shown in Table 1. Our complete observed sample contained candidate lenses that have since been shown to be asterisms, and we do not report those observations here. We split the sample into two subsets based on declination, observing the ten lenses south of declination −10 deg with the ATCA during the 2020 April and 2020 October observing semesters. The remaining fourteen lenses were observed with the VLA during the 20B semester. We describe the observations and analysis for each subset below.

2.1 Australia Telescope Compact Array

Observations were carried out using the 6A and 6B array configurations (maximum baseline 6 km) with two 2048 MHz bands centred on 5.5 and 9 GHz, respectively. This resulted in a synthesized beam with a minor axis of 1.5 arcsec and a major axis that is declination-dependent and typically 3 arcsec (based on −30 deg declination) at 9 GHz. We used the ATCA primary calibrator, PKS 1934–638, to calibrate the bandpass and flux density scale, while appropriate gain calibrators for each source were selected from the ATCA Calibrator Database.[2]

Data were calibrated using standard MIRIAD routines (Sault, Teuben & Wright 1995), with automatic flagging carried out using PGFLAG. Further manual flagging was carried out using BLFLAG where necessary (e.g. particularly bad channels that were not completely flagged with PGFLAG). Observations of the lenses were then imaged using CLEAN, with robust weighting ($R = 0.5$) and a stopping threshold corresponding to approximately 10 times the thermal noise as calculated by INVERT (typically $\lesssim 20$ μJy).

2.2 Karl G. Jansky Very Large Array

Observations were carried out in the A configuration using the *C*-band receiver with one 4096 MHz band centred on 6 GHz, corresponding to a typical angular resolution of 0.3″. To calibrate the bandpass and flux density scale we used observations of 3C286 for targets with right ascensions between 10 and 23 h, and 3C147 for the remaining targets. Gain calibrators for each source were selected from the list of VLA Calibrators.[3] Observations were calibrated using the standard VLA pipeline and then imaged in CASA using TCLEAN with a 50 μJy beam^{-1} threshold for all sources and robust weighting ($R = 0.5$). The resulting images were then corrected for the primary beam using PBCOR. We used AEGEAN (Hancock et al. 2012; Hancock, Trott & Hurley-Walker 2018) with default settings to find the radio sources in each image. We then used CASA IMFIT to fit a Gaussian to all sources in the vicinity of the lens, constraining the centre to within a 10 pixel radius of the AEGEAN source position.

3 RESULTS

We detected radio emission from 12 of 14 VLA targets, and 8 of 10 ATCA targets. None of the 8 targets detected in our ATCA observations were clearly resolved into multiple components, while all but two VLA targets had at least two components detected. Fig. 1 shows images from the VLA lenses with radio emission detected, with each component annotated. Fig. 2 shows the same data overlaid on to optical imaging for reference.

The noise in the VLA images is typically $\lesssim 10$ μJy beam^{-1}, and hence non-detections of images or entire systems can be constrained with a 5σ upper limit of 50 μJy beam^{-1}. The difference in the rate of detection of multiple lensed components between the ATCA and VLA observations is likely due to the maximum baselines of each telescope, which results in our VLA imaging having over five times better angular resolution. Four of the quad lenses observed with the VLA have detectable radio emission from all four components – three of these (GRAL J024848742+191330571, GRAL J060841.42+422936.87, GRAL J181730853+272940139) are known quads with only three components previously detected in optical imaging. All other radio components have been detected previously at other wavelengths.

We find that 11 systems are suitable for Very Long Baseline Interferometry (VLBI) follow-up with either the High Sensitivity Array or the Long Baseline Array (LBA) based on the expected thermal noise achievable with each telescope (4 and 20 μJy beam^{-1}, respectively). We have already observed four of these systems (GRAL J053036−373011, GRAL J081828298−261325078, GRAL J113100−441959, and GRAL J203802−400815) with the LBA and

[2] https://www.narrabri.atnf.csiro.au/calibrators/calibrator_database.html
[3] https://science.nrao.edu/facilities/vla/observing/callist

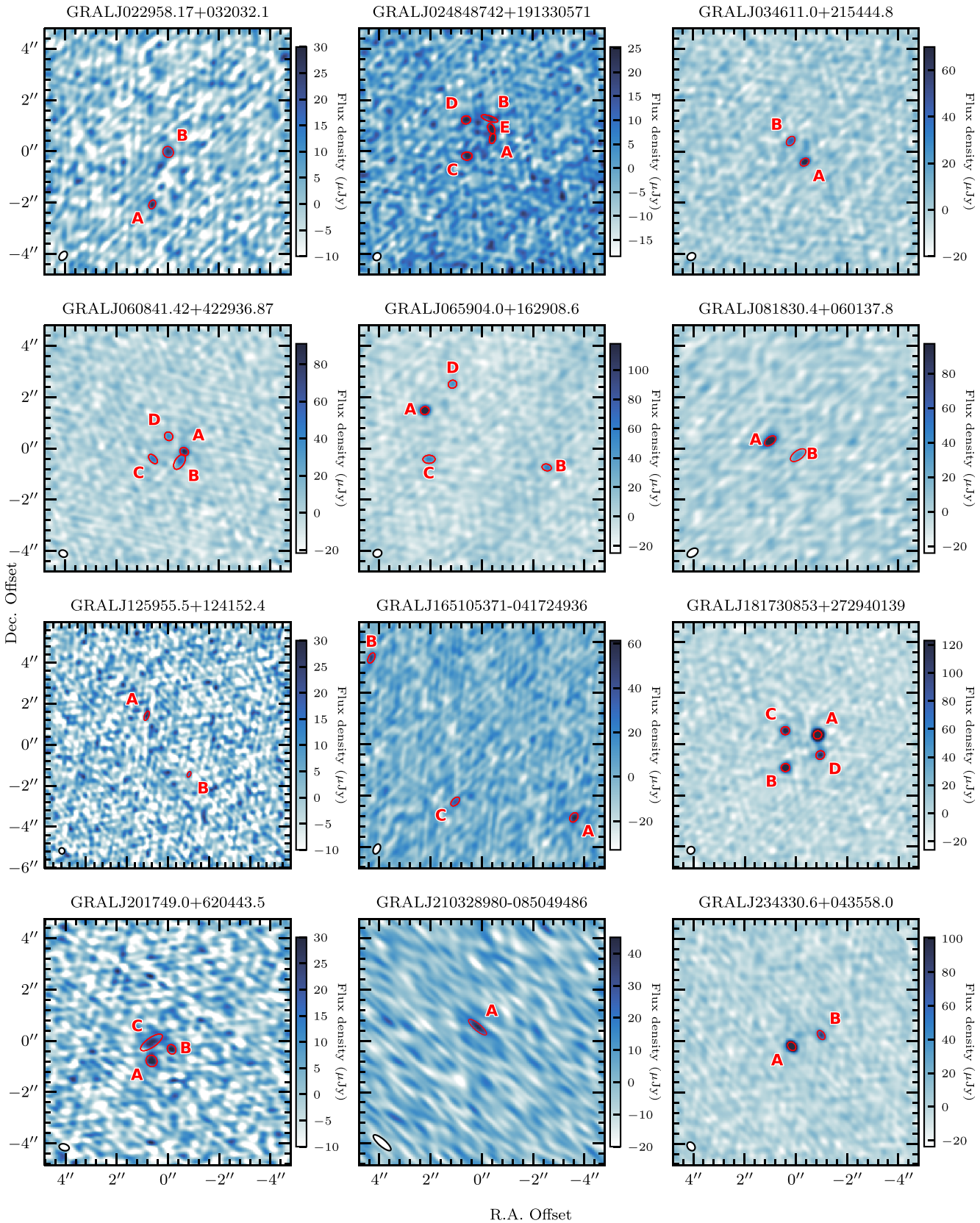

Figure 1. Imaging of lensed systems detected with the VLA at 6 GHz. The ellipse in the bottom left of each panel shows the shape and size of the synthesized beam for that observation. Each component, as measured with IMFIT, is labelled and shown with an overlaid ellipse.

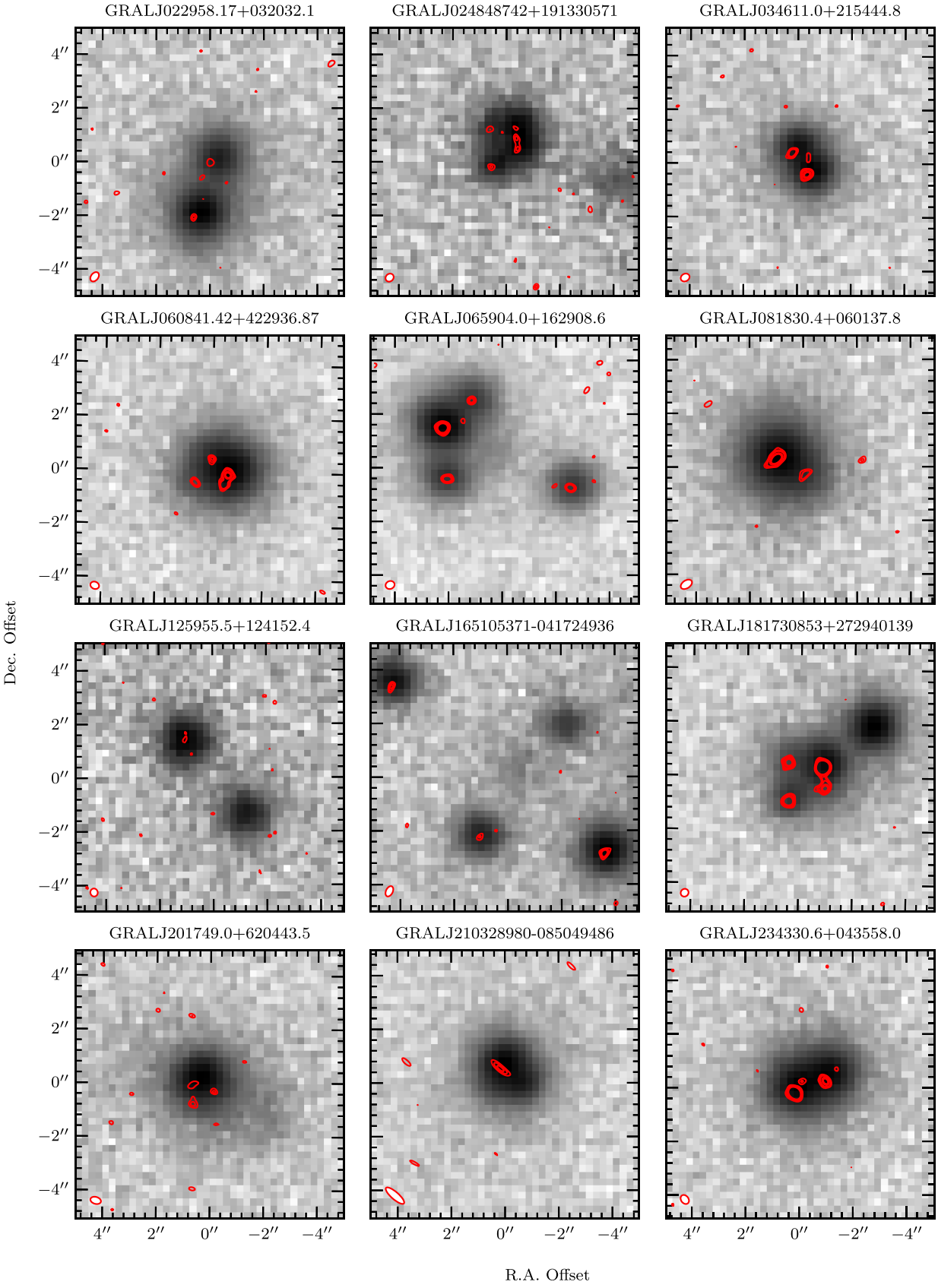

Figure 2. Lensed systems detected with the VLA at 6 GHz. Images are from PanSTARRS with VLA contours (from 25 to 200 μJy in steps of 25 μJy) overlaid. The ellipse in the bottom left of each panel shows the shape and size of the synthesized beam for that radio observation.

these data are currently being analysed, while we plan to observe the remaining nine systems in the future. These results will be presented in future work.

Table 2 shows the observed 5.5 and 9 GHz flux density measurements in our ATCA observations, while Table 3 shows the flux density of each lensed image detected in our VLA observations. For lenses with no components detected, both tables report a 5σ upper limit on the radio emission based on the local noise. Below we discuss selected radio-detected lenses.

3.1 GRAL J024848742+191330571

This quadruply imaged broad absorption line (BAL) quasar at $z = 2.424$ was independently discovered by Delchambre et al. (2019) and Lemon, Auger & McMahon (2019), with spectra first published in Stern et al. (2021). Only three images are present in *Gaia* DR3 but four images are clearly visible in archival data from the Panoramic Survey Telescope and Rapid Response System (Pan-STARRS) and in the *Hubble Space Telescope* (*HST*) images published by Shajib et al. (2019). Our VLA data reveals five components, among which four are roughly compatible with the optical positions, and the fifth one is located between the closest pair of images (labelled *A* and *B* in Fig. 1). The small mismatch ($\sim$0.07 arcsec) between the optical and radio emission of *A* and *B*, and the evidence of a bright fifth component between those images suggest that the background radio source is partly extended and lies very close to the caustic. This extended structure requires higher resolution VLBI observations to be confirmed but is not uncommon among BALs (e.g. Bruni et al. 2013; Kunert-Bajraszewska et al. 2015).

3.2 GRAL J034611.0+215444.8

This sub-arcsecond separation system has been proposed to be a doubly imaged lensed quasar candidate ($z = 2.355$) by Krone-Martins et al. (2019) but as nearly identical quasars (i.e. a system without sufficiently good spectra to be classified as a binary quasar or a lensed system) by Lemon et al. (2023). The *Gaia* DR2 positions and flux ratios are consistent with those observed in the radio. While the lensing galaxy has not yet been detected, the consistency between the radio and optical data (in both astrometry and flux scale) support the lensing hypothesis.

3.3 GRAL J060841.42+422936.87

This source was identified as a lensed quasar candidate based on *Gaia* DR2 where three point-source components were identified. Stern et al. (2021) presented the spectra of two lensed images, demonstrating that the source is a quasar at redshift $z_s = 2.345$. Lemon et al. (2023) spectroscopically confirmed the quad nature of that system. The intervening absorption lines detected at $z > 2.1$ are at a too large redshift to be due to the main deflector, which is not detected in existing imaging data. The triplet of images detected by *Gaia* suggested a fold configuration, as confirmed by the present radio data where four components are clearly detected. A small mismatch of $\sim$0.055 arcsec is observed between the radio and *Gaia* positions and each of the non-merging images (i.e. *C* and *D*), while image *A* agrees with the *Gaia* position to within 0.02 arcsec. This is formally larger than the astrometric uncertainty, and could be an indication for an offset between the optical and radio structures such as a core-shift (e.g. Kovalev, Petrov & Plavin 2017; Pashchenko et al. 2020). Other possible explanations are the presence of a small separation dual acive galactic nuclei (AGN; e.g. Chen et al. 2023), or frequency-dependent delays caused by plasma lensing (e.g. Er & Mao 2022). VLBI imaging across multiple frequencies may help to disentangle these scenarios.

3.4 GRAL J065904044+162908685

This source is a wide separation quad ($\Delta\theta = 5.2$ arcsec) at redshift $z_s = 3.083$ lensed by an early-type galaxy at $z_l = 0.766$ (Stern et al. 2021; Lemon et al. 2023). While only three lensed image positions were listed in *Gaia* DR2, four components are clearly apparent in PanSTARRS images. Four components are also detected with the VLA, with positions in agreement with those from *Gaia*, where available. Despite the relatively low radio luminosity (which classifies this quasar as 'radio-quiet'), the X-ray luminosity is extremely high (Connor et al. 2022).

The faintest radio image (image *D* in Fig. 1) is part of the 'cusp triplet'. While it should approximately be about half as bright as the brightest lensed image (image *A*) based on optical imaging, it is instead a quarter of its brightness. The optical-near-infrared *HST* frames published by Schmidt et al. (2023) also show that image *D* is the faintest image at any wavelength, but the flux ratio with image *A* is never as extreme as in the radio. The lens model proposed by Schmidt et al. (2023) includes a small galaxy visible in the vicinity of this image, and predicts flux ratios in agreement with our radio data. However, the chromatic difference between radio and optical wavelengths may not be explained by the macro model, and suggests the presence of microlensing and/or differential extinction in the optical range.

3.5 GRAL J165105371−041724936

Only the three brightest components of this large separation ($\delta\theta = 10.1$ arcsec) quadruply imaged system, identified in Stern et al. (2021) as a quasar at $z_s = 1.451$ lensed by a galaxy at $z_l = 0.591$, are detected in the VLA data. The undetected fourth image is also the faintest one at optical wavelengths. The optical and radio positions do not match perfectly, with offsets ranging between 0.04 and 0.1 arcsec. This is substantially larger than the astrometric uncertainty, even if considering relative image separation instead of absolute ones. Similar to GRAL J060841.42+422936.87, the origin of this offset could be a core-shift, plasma lensing or a dual AGN (e.g. Kovalev, Petrov & Plavin 2017; Pashchenko et al. 2020; Er & Mao 2022; Chen et al. 2023), and high-resolution VLBI imaging will be required to determine which scenario is occurring.

3.6 GRAL J181730853+272940139

This source was presented as a candidate quadruply imaged quasar by Delchambre et al. (2019), and later confirmed to be a quasar at $z = 3.074$ lensed by an edge-on spiral galaxy (Lemon, Auger & McMahon 2019; Stern et al. 2021). While only three lensed images are detected in *Gaia* data, a fourth faint image is visible in ground-based and *HST* data (Rusu & Lemon 2018; Lemon, Auger & McMahon 2019; Schmidt et al. 2023). This fourth image appears to be strongly reddened at optical wavelengths due to the lensing galaxy, but the optical and radio astrometry agree.

The observed radio flux ratios disagree with the *HST*-based lens model of Schmidt et al. (2023). This may be caused by the presence of a disc-like component in the lensing galaxy which is not included in the model of Schmidt et al. (2023). Such a disc-like component, already proposed for this system in Rusu & Lemon (2018), is known

Table 2. Flux density measurements of the subsample of sources observed with the ATCA. Non-detections are reported with 5σ upper limits. The typical angular resolution is 5 arcsec at 5.5 GHz and 3 arcsec at 9 GHz.

Lens	Flux density (μJy)	
	5.5 GHz	9 GHz
GRAL J024612.2−184505.2	163 ± 14	85 ± 12
GRAL J053036992−373011003	294 ± 18	190 ± 16
GRAL J060710888−215218058	129 ± 20	86 ± 15
GRAL J081828298−261325078	283 ± 20	185 ± 46
GRAL J085911925−301134907	<71	<57
GRAL J113100−441959	186 ± 15	118 ± 15
GRAL J153725327−301017053	122 ± 16	85 ± 14
GRAL J155656.380−135217.292	215 ± 18	129 ± 11
GRAL J201454.1−302452.1	<57	<31
GRAL J203802−400815	333 ± 73	131 ± 35

to produce flux ratio perturbations in other lensed systems (Möller, Hewett & Blain 2003; Hsueh et al. 2018). The presence of a disc in the lens is therefore a good candidate for explaining the radio fluxes. Alternatively, the background source may be intrinsically variable at radio wavelengths. In addition, Connor et al. (2022) note that the X-ray emission is fainter than expected. Further observations are required to distinguish between these competing hypotheses.

3.7 GRAL 201749047+620443509

This system is a compact ($\Delta\theta \sim 0.7$ arcsec) quadruply imaged BAL quasar at $z_s = 1.724$ (Stern et al. 2021). Only three of the quasar images were detected in *Gaia* DR2. The radio data identifies also three components, with one of them (labelled *C* in Fig. 1) slightly extended. A qualitative comparison of the optical and radio data suggests that the extended radio feature could be a blend of two components, i.e. the two images completing the quad in a fold-configuration system, as suggested by Stern et al. (2021). Adaptive optics imaging of this system with the Keck OH- Suppressing Infra-Red Imaging Spectrograph (OSIRIS) resolves out the four lensed images and confirm a fold configuration (Lemon et al. 2023). The pair of fold images is expected to be brighter than images A and B and hence we suspect that the the radio structure is slightly offset with respect to the optical AGN centroid. This like arises from the

Table 3. Flux density and position measurements of lensed images detected with the VLA as reported by CASA IMFIT. Image labels correspond to those seen in Fig. 1. We report the full coordinates for image A and offsets from image A for subsequent images (1σ uncertainties in the final digit are shown in parentheses). Systems with no detections are shown in the bottom section of the table with their 5σ flux density limits.

Lens	Image	R.A.	Decl.	Flux density (μJy)
GRAL J022958.17+032032.1	A	02:29:58.17(7)	+03:20:32.15(7)	30 ± 10
	B	+0.62(3)	−2.05(5)	30 ± 10
GRAL J024848742+191330571	A	02:48:48.7(1)	+19:13:31.33(5)	24 ± 9
	B	−0.12(2)	−0.78(6)	30 ± 10
	C	+0.88(7)	−1.46(4)	30 ± 10
	D	−0.07(3)	−0.4(6)	30 ± 10
	E	+0.91(6)	−0.05(4)	30 ± 10
GRAL J034611.0+215444.8	A	03:46:11.02(3)	+21:54:45.19(3)	50 ± 10
	B	−0.55(2)	−0.82(1)	80 ± 10
GRAL J060841.42+422936.87	A	06:08:41.42(3)	+42:29:37.32(3)	40 ± 10
	B	+0.61(3)	−0.89(3)	50 ± 10
	C	−0.43(3)	−1.0(5)	60 ± 10
	D	−0.61(1)	−0.6(1)	90 ± 10
GRAL J065904.0+162908.6	A	06:59:4.08(3)	+16:29:11.09(2)	50 ± 10
	B	+0.92(4)	−2.93(2)	60 ± 10
	C	−3.68(2)	−3.25(1)	60 ± 10
	D	+1.078(7)	−1.029(7)	190 ± 10
GRAL J081830.4+060137.8	A	08:18:30.4(8)	+06:01:37.52(6)	40 ± 10
	B	+1.09(1)	+0.56(1)	130 ± 10
GRAL J125955.5+124152.4	A	12:59:55.47(3)	+12:41:50.96(6)	20 ± 7
	B	+2.07(4)	+2.86(8)	29 ± 9
GRAL J165105371-041724936	A	16:51:5.45(4)	−04:17:27.16(4)	40 ± 10
	B	+3.27(2)	+5.6(4)	50 ± 10
	C	−4.63(2)	−0.62(2)	60 ± 10
GRAL J181730853+272940139	A	18:17:30.78(1)	+27:29:39.74(1)	120 ± 10
	B	+1.36(1)	+0.949(9)	140 ± 10
	C	+1.359(7)	−0.491(6)	190 ± 10
	D	+0.103(2)	+0.787(2)	530 ± 10
GRAL J201749.0+620443.5	A	20:17:49.1(1)	+62:04:43.5(1)	28 ± 9
	B	−0.78(4)	−0.27(5)	30 ± 10
	C	−0.0(5)	−0.72(6)	30 ± 10
GRAL J210328980−085049486	A	21:03:28.99(8)	−08:50:48.93(7)	44 ± 9
GRAL J234330.6+043558.0	A	23:43:30.55(1)	+04:35:58.25(2)	90 ± 10
	B	+1.148(5)	−0.437(5)	280 ± 10
GRAL J090710.5+000321.2				<40
GRAL J220015.55+144859.5				<50

Table 4. Model parameters for selected lenses.

Name	θ_E (arcsec)	e	PA$_e$ (deg)	γ	θ_γ (deg)	χ^2_{ima}	χ^2_{tot}	χ^2_{gal}
GRAL J024848.7+191330	0.739	0.502	2.77	0.252	85.04	0.26	0.24	0.02
GRAL J060841.4+422937[a]	0.621	0.180	18.31	–	–	0.08	0.08	–
GRAL J065904.1+162909	2.408	0.454	1.91	0.128	−63.5	0.56	0.33	0.23
GRAL J181730.8+272940	0.899	0.579	55.94	0.126	−28.6	0.15	0.01	0.14

[a]SIE model, without shear.

BAL nature of this quasar – an extended structure is inferred in another BAL in this sample (GRAL J024848742+191330571). Such extended radio emission is often detected in high-resolution radio data of BALs (e.g. Bruni et al. 2013; Kunert-Bajraszewska et al. 2015). The small apparent mismatch between the absolute optical and radio position may further support this interpretation, although this mismatch is tentative, due to the potentially larger error on the absolute astrometry.

3.8 GRAL J234330.6+043558.0

This system is a doubly imaged lensed quasar at $z_s = 1.604$ discovered by Krone-Martins et al. (2019). While the lens has not been directly detected, narrow absorption features at $z_l = 0.855$ provide a plausible lens redshift. The radio and optical positions are in excellent agreement, while the flux ratios differ by more than a factor of two. An optical flux ratio of 0.778 is measured, while a ratio of 0.306 is measured in the radio. This might be explained by intrinsic variability of the source, by microlensing affecting the optical wavelengths, or by dust extinction. The difference of colour of the two images in the optical data suggests that microlensing and/or dust reddening may play a role.

3.9 Marginal detections/other systems

Several systems show either detection of only one lensed image, or very faint detections. We briefly discuss those systems hereafter:

(i) GRAL J022958.17+032032.1: This system was noted by Krone-Martins et al. (2019) as a doubly imaged lensed quasar candidate with two components separated by 2.14 arcsec. Due to the difference in the shape of the Mg II emission in the spectra of the two quasar images, and the absence of detection of a lensing galaxy, Lemon et al. (2020) argue that the system is more likely to be a binary. The radio detection of the two images shows that the two quasars spectral energy distributions may be similar up to the radio domain.Hence, additional data may yet be needed to rule out the lensing hypothesis. The astrometry of the two radio images is compatible with that of *Gaia* DR2, but remains tentative as the radio flux is only marginally above the noise.

(ii) GRAL J125955.5+124152.4: The lensed nature of this wide separation ($\Delta\theta = 3.5$ arcsec) system (Hennawi et al. 2006; Foreman, Volonteri & Dotti 2009; Krone-Martins et al. 2019) composed of two quasar images at $z_s = 2.196$ is not certain. Radio emission compatible with the optical positions is tentatively detected, but at low significance.

(iii) GRAL J210328980-085049486: Only one radio component is identified for this compact ($\Delta\theta < 1.0$ arcsec) quadruply imaged quasar at $z_s = 2.446$. The radio emission matches the brightest of the triplet of point-source emission detected in *Gaia* DR2 (Delchambre et al. 2019; Stern et al. 2021). The non-detection of the other two components is compatible with their expected fainter flux based on the observed optical flux ratios. The strong elongation of the radio beam does not enable us to test whether the radio component results from the merging of two point-sources, and/or is due exclusively to point-like radio emission.

4 LENS MODELLING

We have performed simple lens modelling using the public modelling software LENSMODEL (Keeton 2001). The observational constraints result from the combination of our radio data with archival optical imaging to constrain the lensing galaxy position. The relative position of the lensing galaxy has been obtained with respect to the brightest lensed image by matching the existing *HST* imaging to our VLA data. Supported by the finding that some small mismatches (<10 mas) between radio and optical astrometry could arise due to there being physically different optical/radio emitting regions, we have assumed a uniform 20 mas uncertainty on all lens positions. The observables that we aim to reproduce are the lensed image positions, and the position of the lensing galaxy where known. The mass distribution of the lens is parametrized as a singular isothermal ellipsoid (SIE). This model has the following parameters: the Einstein radius, θ_E; the two-dimensional lens position (x_g, y_g); the ellipticity, $e = 1 - q$ (where q is minor to major axis ratio of the SIE, i.e. $q = b/a$); and the position angle of the major axis of the mass distribution, θ_e. The tidal contribution from the mass distribution external to the main lens is parametrized with a shear term characterized by an amplitude γ and a position angle θ_γ (measured East of North and pointing towards the mass producing the shear). The results of these fits are shown in Table 4 and in Fig. 3.

4.1 GRAL J024848.7+191330

The VLA images positions can be reproduced by a SIE+shear model centroid compatible with the optical position (within the 0.02 arcsec astrometric uncertainty). The best model is found for an unrealistically large ellipticity ($e = 0.54$) and external shear ($\gamma_{ext} = 0.29$). An exploration of the seven-dimensional parameter space reveals that two other local minima characterized by a slightly higher reduced χ^2 (but lower than 1) exist. They both correspond to a rounder mass distribution and lower shear. If we set a prior on the alignment between the lens and light mass such that $|\phi_{light} - \phi_{mass}| < 20$ deg (as suggested by numerous lensing studies, e.g. Sluse et al. 2012; Bruderer et al. 2016), we find a slightly rounder model yet characterized by a very large shear amplitude. Our lens model parameters are compatible with those obtained by Schmidt et al. (2023) using *HST* imaging. The small axis ratio $q = b/a \sim 0.5$ of the mass distribution may be physical as the lens light also displays a low value of $q = 0.44$. The large inferred shear may be an artefact caused by choice of a purely elliptical mass distribution. A discy (and/or boxy) component is likely to be present in the galaxy, but its absence from the model may be captured by the shear term

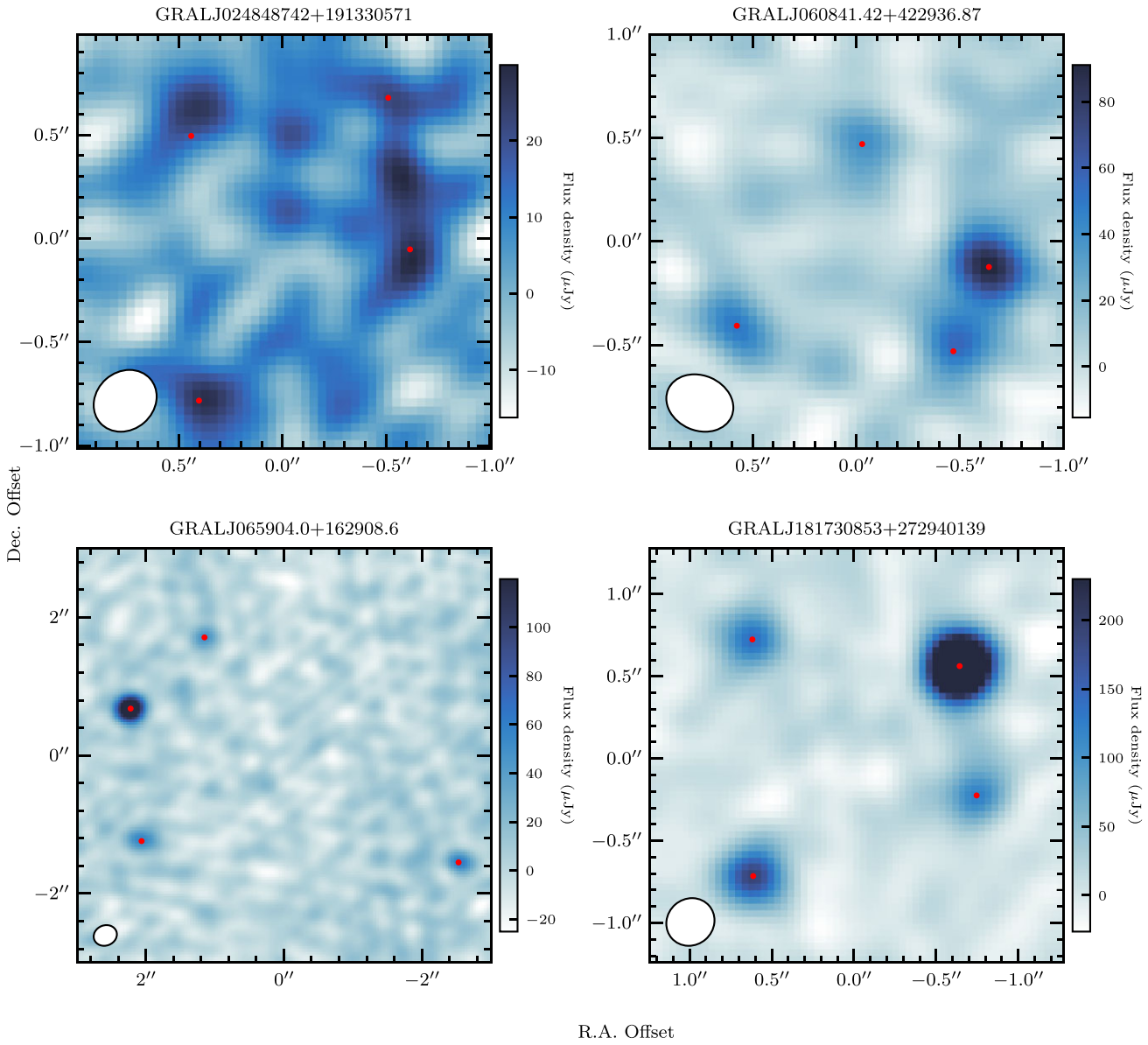

Figure 3. VLA imaging of selected lenses at 6 GHz with modelled image positions overlaid. These cutouts are zoomed and re-centred compared to Fig. 1. Table 4 details the model parameters for each system. The ellipse in the bottom left of each panel shows the shape and size of the synthesized beam for that observation.

(Van de Vyvere et al. 2022a; Etherington et al. 2023). Other types of angular structures can also potentially play a role (Van de Vyvere et al. 2022b). Nevertheless, we do not exclude that a fraction of this large shear is effectively related to the lens environment, and produced by the bright galaxies visible in optical images within 1 arcmin of the lens.

4.2 GRAL J060841.4+422937

For this system we have simplified our model due to the large uncertainty on the position of the fourth radio lensed image. We have modelled the image positions using an SIE (i.e. no added shear), leaving the position of the lensing galaxy as a free parameter. The new lens model is substantially different from the one inferred from the triplet of *Gaia* images by Stern et al. (2021). The main difference occurs for the predicted position of the lensing galaxy which differs by 0.3 arcsec compared to the previous model. Such a change is not unexpected as a triplet of images does not fully constrain a simple SIE (Luhtaru, Schechter & de Soto 2021). The predicted flux ratio between the pair of fold images is close to 1:1, as expected asymptotically for fold images. The radio measurement yields a ratio A/B $\sim$ 4:5 which is consistent with the expected 1:1 ratio within uncertainties.

4.3 GRAL J065904.1+162909

Our simple SIE+shear model successfully fits the radio positions within the uncertainties. The derived shape of the mass distribution of the lensing galaxy however deviates substantially from the shape of the luminosity profile (e, ϕ_L) = (0.95, -27.8 deg) derived by Schmidt et al. (2023). Our model requires a flatter profile (e =

0.45), with a major axis position angle offset by about 30 deg compared to the light. The likely reason for this discrepancy is the object detected in *HST* images in the vicinity of image *D*, and which is not included in our simple model. The model proposed by Schmidt et al. (2023), which is constrained by extended images of the quasar host and accounts for the companion, yields a better agreement between the shapes of the lens light and mass profiles.

4.4 GRAL J181730.8+272940

We find that a simple SIE+shear model of this system is able to reproduce the VLA image positions within the uncertainties. The modelled position of the lens centroid is offset from the known optical position by ∼0.1 arcsec (Schmidt et al. 2023). This small discrepancy is not unexpected given the uncertainties on the relative astrometry, the presence of dust in the optical regime, and the possibility that the radio and optical emission do not share a common origin.

The derived mass distribution is very flattened ($q = 0.42$) but rounder than the light ($q_L = 0.26$). The position angle of the light and mass also seem to agree reasonably well, within about 10 deg. While such a mass distribution is not at odds with the spiral nature of the lens, we note that the inferred shear is large and almost aligned with the position angle of the mass ($\Delta\phi = 6.5$ deg). As in the case of GRAL J024848.7+191330, this may be caused by 'discyness', 'boxyness', or ellipticity gradients in the true mass distribution but not accounted for by the model (Van de Vyvere et al. 2022a, b; Etherington et al. 2023).

Our modelling yields an Einstein radius consistent with that measured by Schmidt et al. (2023), but the amplitude and orientation of the ellipticity and shear differ between the two models. The origin of this discrepancy is not clear, but may be related to the use of a prior on the relative orientation of the major axis of the light and mass distribution of the lens by Schmidt et al. (2023).

5 CONCLUSIONS

In this work, we have presented radio observations of 24 strongly lensed systems from the GraL project with the ATCA and the Karl G. Jansky VLA. VLA observations were carried out at 6 GHz, while the ATCA data are centred on 5.5 and 9 GHz and both sets of observations achieved a typical 5σ sensitivity of approximately 50 μJy. We detected radio emission from 20 lensed systems in total, including 11 with radio emission detected from multiple lensed images. The ATCA observations provide imaging with a typical spatial resolution of 3 arcsec, which is not sufficient to resolve the individual lensed images of any of the 13 systems targeted with that facility. Almost half of the targeted systems are known quadruply imaged quasars. Six of them display unresolved emission above 100 μJy at 5 GHz, four have their four lensed images detected, two have three images detected, and one has only its brightest image detected. The systems for which only upper limits on the radio flux density have been obtained are all doubly imaged quasars.

The two broad absorption line quasars detected in our VLA observations (GRAL J024848742+191330571 and GRAL J201749047+620443509) show evidence for extended emission. Extended radio emission has previously been detected in the two other quadruply imaged BALs observed in the radio domain, PG1115+080 (Hartley et al. 2021) and H1413+117 (Kayser et al. 1990; Zhang et al. 2022). The origin of such emission is likely related to wind–interstellar medium interaction and is commonly observed in BAL quasars (Bruni et al. 2013; Kunert-Bajraszewska et al. 2015). Gravitationally lensed BALs provide an exceptional laboratory for studying this phenomenon at high spatial resolution owing to natural lensing magnification (e.g. Zhang et al. 2022).

The VLA astrometry provides high-precision relative lensed images positions which nicely complement *Gaia* astrometry. We have built new lens models constrained by radio astrometry for the systems with incomplete *Gaia* astrometry. Guided by lens models, and comparing optical and radio flux ratios, we have searched for anomalies among the relative fluxes of the quadruply imaged components. Differences between the lens model and the data can potentially be the signature for the presence of dark matter substructures in the lens (e.g. Xu et al. 2015). We found an anomaly in GRAL J181730.8+272940 but it is likely caused by the presence of a disc-like component in the lens that is not included in the model. The anomaly found in GRAL J065904.1+162909 is most likely due to a small galaxy detected in the *HST* images. This latter system, together with GRAL J234330.6+043558.0 (a doubly imaged quasar), also show a substantially different flux ratio at optical and radio wavelengths. The latter may be explained by the presence of microlensing or dust extinction in the optical range (e.g. Wambsganss & Paczynski 1991; Schechter & Wambsganss 2002).

We have performed the first systematic comparison of the relative quasar image positions at optical and radio wavelengths for a sample of lensed systems, enabled by the high-precision astrometry provided by *Gaia* and our VLA imaging. We detect a mistmatch (sometimes tentatively) for four systems, including the two BALs. For the two other systems, i.e. GRAL J060841.42+422936.87 and GRAL J165105371−041724936, this mismatch could be the signature of a core shift, i.e. an offset between the emission arising from the accretion disc and from the base of the jet (Kovalev, Petrov & Plavin 2017; Pashchenko et al. 2020). The origin may be different for the two BALs for which extended radio emission appears to be present.

ACKNOWLEDGEMENTS

Parts of this research were conducted by the Australian Research Council Centre of Excellence for Gravitational Wave Discovery (OzGrav), project number CE170100004.

DS acknowledges the support of the Fonds de la Recherche Scientifique-FNRS, Belgium, under grant No. 4.4503.1.

The work of DS and TC was carried out at the Jet Propulsion Laboratory, California Institute of Technology, under a contract with the National Aeronautics and Space Administration (80NM0018D0004).

The Australia Telescope Compact Array is part of the Australia Telescope National Facility which was funded by the Australian Government for operation as a National Facility managed by CSIRO. We acknowledge the Gomeroi people as the traditional owners of the Observatory site.

This research has made use of NASA's Astrophysics Data System Bibliographic Services.

This work presents results from the European Space Agency (ESA) space mission *Gaia*. *Gaia* data are being processed by the *Gaia* Data Processing and Analysis Consortium (DPAC). Funding for the DPAC was provided by national institutions, in particular the institutions participating in the *Gaia* MultiLateral Agreement (MLA). The *Gaia* mission website is https://www.cosmos.esa.int/gaia. The *Gaia* archive website is https://archives.esac.esa.int/gaia.

This work benefitted from the existence of the gravitational lens data bases of Ducourant et al. (2018) and Lemon, Auger & McMahon (2019).

DATA AVAILABILITY

The VLA visibilities used in this work can be accessed via the NRAO Archive (https://data.nrao.edu/portal/) under project 20B-363. The ATCA visibilities used in this work can be accesed via the Australia Telescope Online Archive (https://atoa.atnf.csiro.au/) under projects C3371 and CX449. All other data underlying this article will be shared on reasonable request to the corresponding author.

REFERENCES

Biggs A. D., 2021, MNRAS, 505, 2610
Browne I. W. A. et al., 2003, MNRAS, 341, 13
Bruderer C., Read J. I., Coles J. P., Leier D., Falco E. E., Ferreras I., Saha P., 2016, MNRAS, 456, 870
Bruni G., Dallacasa D., Mack K. H., Montenegro-Montes F. M., González-Serrano J. I., Holt J., Jiménez-Luján F., 2013, A&A, 554, A94
Chen Y.-C., Liu X., Lazio J., Breiding P., Burke-Spolaor S., Hwang H.-C., Shen Y., Zakamska N. L., 2023, ApJ, 958, 29
Connor T. et al., 2022, ApJ, 927, 45
Delchambre L. et al., 2019, A&A, 622, A165
Ducourant C. et al., 2018, A&A, 618, A56
Er X., Mao S., 2022, MNRAS, 516, 2218
Etherington A. et al., 2023, preprint (arXiv:2301.05244)
Foreman G., Volonteri M., Dotti M., 2009, ApJ, 693, 1554
Hancock P. J., Murphy T., Gaensler B. M., Hopkins A., Curran J. R., 2012, MNRAS, 422, 1812
Hancock P. J., Trott C. M., Hurley-Walker N., 2018, Publ. Astron. Soc. Aust., 35, e011
Hartley P., Jackson N., Sluse D., Stacey H. R., Vives-Arias H., 2019, MNRAS, 485, 3009
Hartley P., Jackson N., Badole S., McKean J. P., Sluse D., Vives-Arias H., 2021, MNRAS, 508, 4625
Hennawi J. F. et al., 2006, AJ, 131, 1
Hsueh J.-W., Despali G., Vegetti S., Xu D., Fassnacht C. D., Metcalf R. B., 2018, MNRAS, 475, 2438
Hsueh J. W., Enzi W., Vegetti S., Auger M. W., Fassnacht C. D., Despali G., Koopmans L. V. E., McKean J. P., 2020, MNRAS, 492, 3047
Jackson N., Tagore A. S., Roberts C., Sluse D., Stacey H., Vives-Arias H., Wucknitz O., Volino F., 2015, MNRAS, 454, 287
Kayser R., Surdej J., Condon J. J., Kellermann K. I., Magain P., Remy M., Smette A., 1990, ApJ, 364, 15
Keeton C. R., 2001, preprint(astro–ph/0102340)
Kellermann K. I., Condon J. J., Kimball A. E., Perley R. A., Ivezić Ž., 2016, ApJ, 831, 168
Kovalev Y. Y., Petrov L., Plavin A. V., 2017, A&A, 598, L1
Krone-Martins A. et al., 2018, A&A, 616, L11
Krone-Martins A. et al., 2019, preprint (arXiv:1912.08977)
Kunert-Bajraszewska M., Cegłowski M., Katarzyński K., Roskowiński C., 2015, A&A, 579, A109
Lemon C. A., Auger M. W., McMahon R. G., 2019, MNRAS, 483, 4242
Lemon C. et al., 2020, MNRAS, 494, 3491
Lemon C. et al., 2023, MNRAS, 520, 3305
Luhtaru R., Schechter P. L., de Soto K. M., 2021, ApJ, 915, 4
MacLeod C. L., Jones R., Agol E., Kochanek C. S., 2013, ApJ, 773, 35
Mangat C. S., McKean J. P., Brilenkov R., Hartley P., Stacey H. R., Vegetti S., Wen D., 2021, MNRAS, 508, L64
Möller O., Hewett P., Blain A. W., 2003, MNRAS, 345, 1
Pashchenko I. N., Plavin A. V., Kutkin A. M., Kovalev Y. Y., 2020, MNRAS, 499, 4515
Powell D. M., Vegetti S., McKean J. P., Spingola C., Stacey H. R., Fassnacht C. D., 2022, MNRAS, 516, 1808
Rusu C. E., Lemon C. A., 2018, Res. Notes Am. Astron. Soc., 2, 187
Sault R. J., Teuben P. J., Wright M. C. H., 1995, in Shaw R. A., Payne H. E., Hayes J. J. E.eds, ASP Conf. Ser., Vol.77, Astronomical Data Analysis Software and Systems IV. Astron. Soc. Pac., San Francisco, p. 433
Schechter P. L., Wambsganss J., 2002, ApJ, 580, 685
Schmidt T. et al., 2023, MNRAS, 518, 1260
Shajib A. J. et al., 2019, MNRAS, 483, 5649
Sluse D., Chantry V., Magain P., Courbin F., Meylan G., 2012, A&A, 538, A99
Stern D. et al., 2021, ApJ, 921, 42
Suyu S. H. et al., 2012, ApJ, 750, 10
Van de Vyvere L., Gomer M. R., Sluse D., Xu D., Birrer S., Galan A., Vernardos G., 2022a, A&A, 659, A127
Van de Vyvere L., Sluse D., Gomer M. R., Mukherjee S., 2022b, A&A, 663, A179
Wambsganss J., 1990, PhD thesis, Ludwig-Maximilians-Univ. Munich (Germany)
Wambsganss J., 2006, in Meylan G., Jetzer P., North P., Schneider P., Kochanek C. S., Wambsganss J.eds, Saas-Fee Advanced Course 33: Gravitational Lensing: Strong, Weak and Micro. Springer-Verlag, Berlin, p. 453
Wambsganss J., Paczynski B., 1991, AJ, 102, 864
Wertz O. et al., 2019, A&A, 628, A17
Xu D., Sluse D., Gao L., Wang J., Frenk C., Mao S., Schneider P., Springel V., 2015, MNRAS, 447, 3189
Zhang L. et al., 2022, MNRAS, 524, 3671

[1]*Centre for Astrophysics and Supercomputing, Swinburne University of Technology, Hawthorn, Victoria, 3122, Australia*
[2]*ARC Centre of Excellence for Gravitational Wave Discovery (OzGrav), Hawthorn, Victoria, 3122, Australia*
[3]*Space Sciences, Technologies and Astrophysics Research (STAR) Institute, University of Liège, Liege, 4000, Belgium*
[4]*Sydney Institute for Astronomy, School of Physics, The University of Sydney, Camperdown, NSW 2006, Australia*
[5]*Donald Bren School of Information and Computer Sciences, University of California, Irvine, CA 92697, USA*
[6]*CENTRA/SIM, Faculdade de Ciɔencias, Universidade de Lisboa, Ed. C8, Campo Grande, P-1749-016 Lisboa, Portugal*
[7]*Jet Propulsion Laboratory, California Institute of Technology, 4800 Oak Grove Drive, Pasadena, CA 91109, USA*
[8]*Division of Physics, Mathematics, and Astronomy, Caltech, Pasadena, CA 91125, USA*
[9]*Université Côte d'Azur, Observatoire de la Côte d'Azur, CNRS, Laboratoire Lagrange, Bd de l'Observatoire, CS 34229, F-06304 Nice cedex 4, France*
[10]*Center for Astrophysics|Harvard & Smithsonian, 60 Garden St, 02138 Cambridge, MA, USA*
[11]*Instituto de Astronomia, Geofísica e Ciências Atmosféricas, Universidade de São Paulo, Rua do Matão, 1226, Cidade Universitária, 05508-900 São Paulo, SP, Brazil*
[12]*Laboratoire d'Astrophysique de Bordeaux, Univ. Bordeaux, CNRS, B18N, Allée Geoffroy Saint-Hilaire, F-33615 Pessac, France*
[13]*Center for Theoretical Physics, Polish Academy of Sciences, Warsaw 01-224, Poland*
[14]*Lohrmann-Observatorium, Technische Universität Dresden, D-01062 Dresden, Germany*
[15]*Department of Physics and Astronomy, Louisiana State University, Baton Rouge, LA 70803, USA*
[16]*Aryabhatta Research Institute of Observational Sciences (ARIES), Manora Peak, Nainital 263002, India*
[17]*Departamento de Física – CCET, Universidade Federal de Sergipe, Rod. Marechal Rondon s/n, 49.100-000, Jardim Rosa Elze, São Cristóvão, SE, Brazil*
[18]*Centre for Astrophysics Research, University of Hertfordshire, College Lane, Hatfield, AL10 9AB, UK*
[19]*Astronomisches Rechen-Institut (ARI), Zentrum für Astronomie der Universität Heidelberg (ZAH), Mönchhofstr. 12-14, D-69120 Heidelberg, Germany*

This paper has been typeset from a TEX/LATEX file prepared by the author.